Check for updates

RESEARCH ARTICLE

NANO · MICRO small
www.small-journal.com

Interfacial Growth of Large Area Single-Crystalline Silver Sheets Through Ambient Microdroplets

Depanjan Sarkar, Anirban Som, Keerthana Unni, Sujan Manna, and Pradeep Thalappil**

This article is dedicated to Professor Pulickel M. Ajayan.

The creation of micrometer-sized sheets of silver at the air–water interface by direct deposition of electrospray-generated silver ions (Ag^+) on an aqueous dispersion of reduced graphene oxide (RGO), in ambient conditions, is reported. In the process of electrospray deposition (ESD), an electrohydrodynamic flow is created in the aqueous dispersion, and the graphene sheets assemble, forming a thin film at the air–water interface. The deposited Ag^+ coalesce to make single-crystalline Ag sheets on top of this assembled graphene layer. Fast neutralization of Ag^+ forming atomic Ag, combined with their enhanced mobility on graphene surfaces, presumably facilitates the growth of larger Ag clusters. Moreover, restrictions imposed by the interface drive the crystal growth in 2D. By controlling the precursor salt concentration, RGO concentration, deposition time, and ion current, the dimensionality of the Ag sheets can be tuned. These Ag sheets are effective substrates for surface-enhanced Raman spectroscopy (SERS), as demonstrated by the successful detection of methylene blue at nanomolar concentrations.

1. Introduction

Electrospray deposition (ESD) is a method wherein charged droplet sprays are placed onto a surface. Initially employed as a preparative tool in nuclear research,[1] ESD has progressed into a precise deposition technique applied in various domains. These applications encompass the development of polymer coatings,[2] the creation of thin conductive ceramic films,[3] and even the preparation of films involving DNA,[3] and proteins.[4] Recently, ambient ESD has emerged as an innovative synthetic method for producing a diverse range of nanomaterials.[5] In this process, solvated ions present in a droplet plume undergo reduction to create nanoparticles, which are then deposited onto an electrically grounded surface. This technique offers the advantage of avoiding the use of harsh reducing agents. Notably, recent research from our team has demonstrated the capability of ESD in synthesizing nanomaterials, with the resulting material's dimensional characteristics influenced by the nature of the deposition surface. For example, while ESD of silver and silver–palladium mixture on wire mesh resulted in 1D nanowires,[6] deposition of palladium on air–water interface formed 2D nanoparticle–nanosheets.[7]

Interfacial processes have been at the forefront of producing extensive 2D assemblies for many years. In these processes, molecules or particles are confined at the interfaces between liquid and air or between two liquids, allowing them to form assemblies solely in the 2D plane along the interface. A similar approach has proven successful in the bottom–up synthesis of both inorganic and organic 2D materials.[8] In these processes, the components undergo reactions at an interface, resulting in the formation of 2D structures.[9] Taking inspiration from these methods, we attempted the ESD of Ag^+ ions at air–water interfaces. This process led to the creation of Ag nanoparticle–nanosheets (NP–NS), a pseudo-nanosheet where tiny Ag nanoparticles formed through ESD were assembled in a 2D arrangement.[7] We hypothesized that the restricted mobility of the formed Ag nanoparticles prevents them from merging into genuine 2D structures.

Graphene, a well-known nanomaterial, is famous for its unusual electronic and mechanical properties.[10–16] Bonding,[17] transport,[18] diffusion,[19,20] and aggregation of metals [21] on graphene have been extensively studied producing rich science and relevant applications. Extensive research has been conducted to investigate the increased mobility of various metals and metal clusters on graphene surfaces.[22] According to computational studies, small clusters of gold (Au) and silver (Ag) have a preference for adopting 2D structures on graphene surfaces. Additionally, at higher concentrations, these clusters tend to form islands on the graphene surface.[23,24] An earlier report from our group showed the coalescence of monolayer-protected Au clusters on graphene surfaces due to their enhanced mobility.[25]

D. Sarkar, A. Som, K. Unni, S. Manna, P. Thalappil
DST Unit of Nanoscience (DST UNS) and Thematic Unit of Excellence (TUE)
Department of Chemistry
Indian Institute of Technology Madras
Chennai 60036, India
E-mail: depanjan_coe@icsrpis.iitm.ac.in; pradeep@iitm.ac.in
D. Sarkar, A. Som, K. Unni, S. Manna, P. Thalappil
Centre of Excellence on Molecular Materials and Functions
Department of Chemistry
Indian Institute of Technology Madras
Chennai 60036, India

The ORCID identification number(s) for the author(s) of this article can be found under https://doi.org/10.1002/smll.202400159

DOI: 10.1002/smll.202400159

 © 2024 Wiley-VCH GmbH

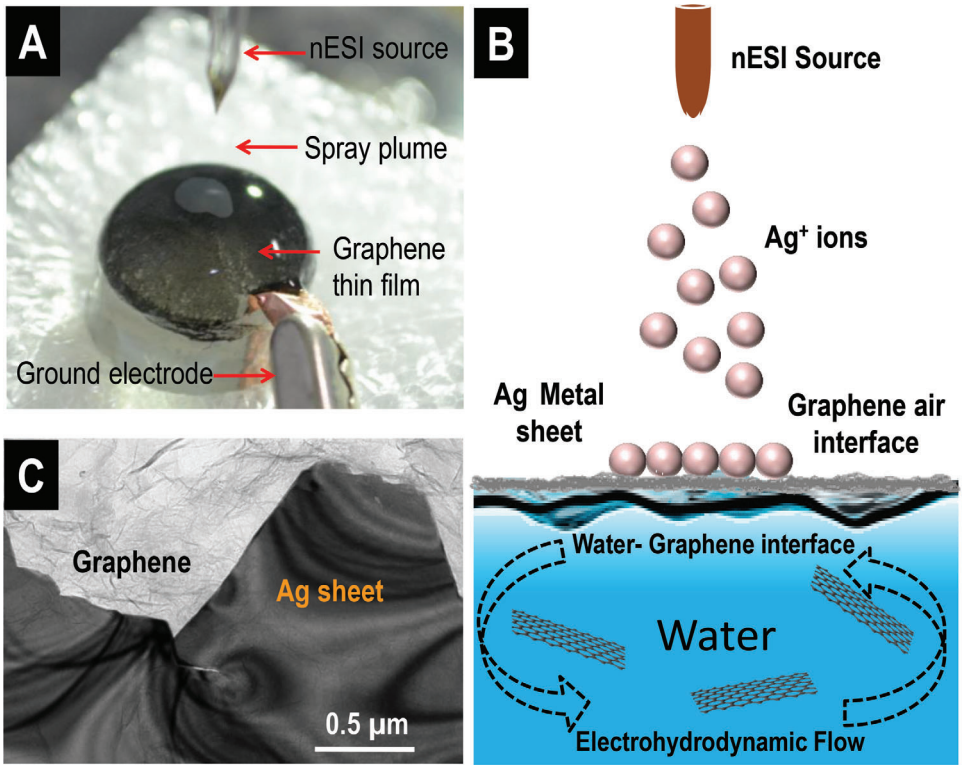

Figure 1. A) Optical micrograph of the electrospray deposition setup, showcasing the formation of a graphene thin film at the air–water interface following ESD onto an aqueous graphene suspension. B) Schematic representation of the ESD process, illustrating the electrohydrodynamic flow within the aqueous RGO suspension, leading to the formation of a thin film at the liquid surface, followed by the deposition of a silver sheet onto the RGO layer, and C) TEM image of the deposited solid silver sheet on the RGO film.

These inspired us to introduce graphene into our ESD synthetic system.

In this work, we successfully achieved the formation of large-area single crystalline silver sheets, measuring hundreds of micrometers in length, on an aqueous suspension of graphene under ambient conditions. Our approach combines several key factors: the ambient ESD method generates tiny silver clusters, the enhanced mobility of these clusters on graphene allows them to coalesce into larger structures, and the presence of an interface restricts their growth in 2D. While various methods exist to fabricate 2D silver sheets with controlled dimensions, such as cathodic arc deposition and magnetron sputtering,[26–29] they necessitate demanding conditions like high vacuum, elevated temperature, and involvement of specific environments, besides appropriate equipment. Furthermore, these techniques convert existing silver metal into the desired 2D form. In contrast, our straightforward process eliminates the need for specialized chemicals or complex instruments. Instead, it transforms a readily available salt solution into single-crystalline metallic sheets under ambient conditions. This chemical approach with minimum infrastructure offers a significant advantage in terms of simplicity and accessibility. Besides, it extends the scope of ambient synthesis in microdroplets, an active subject area in the context of molecular science.[30,31] We have extensively characterized these Ag sheets using microscopic and spectroscopic techniques and studied their growth dynamics. The resulting Ag sheets demonstrated excellent SERS activity, making them highly promising for potential applications in sensing various contaminations.

2. Results and Discussion

2.1. Synthesis of Ag-Sheets using ESD

Figure 1A presents an optical image of the ESD apparatus and the formation of an RGO film on the top of the water surface. Initially, the electrospray deposition of the Ag-salt solution induced an electrohydrodynamic flow that led to the creation of a thin layer of assembled RGO at the air–water interface. As the process continues, the subsequent ESD of Ag^+ ions onto the RGO layer facilitates the neutralization of these ions into Ag atoms, and further, enables the coalescence of Ag atoms to form the desired metal sheets. Formation of the assembled RGO layer is facilitated by ESD-induced electrohydrodynamic motion in the aqueous RGO dispersion. This entire process is schematically presented in Figure 1B. In a previous report, we demonstrated a similar electrohydrodynamic flow in pure water to assemble suspended Pd nanoparticles on its surface, leading to the formation of NP–NS.

To establish that the formation of the RGO layer on the water surface was driven by similar forces, control experiments were performed. In such experiments, only DI water was electrosprayed onto an aqueous suspension of RGO. The assembled RGO film was collected on a glass coverslip (Figure S1A,

© 2024 Wiley-VCH GmbH

16136829, 0, Downloaded from https://onlinelibrary.wiley.com/doi/10.1002/smll.202400159 by Central Library, Wiley Online Library on [22/05/2024]. See the Terms and Conditions (https://onlinelibrary.wiley.com/terms-and-conditions) on Wiley Online Library for rules of use; OA articles are governed by the applicable Creative Commons License

Supporting Information) and placed on a sheet of paper with letters A, B, & C written using a red marker pen. The letters were clearly visible after placing the RGO-coated cover slip on top of them, indicating the thinness of the film. The RGO layers appear to be closely packed by the electrohydrodynamic flow to form the thin layer, as evidenced by the electrical continuity (Figure S1B, Supporting Information) of the RGO film-coated coverslips. Figure S1C (Supporting Information) schematically depicts the process of RGO assembly at the water surface and the subsequent formation of a metallic Ag sheet on top of it.

In the case of ESD of Ag^+ ions, a shiny white round spot with a metallic luster was observed just under the sprayer head on the RGO surface after continued deposition for 2 h. This material was collected on various substrates such as transmission electron microscope (TEM) grids, indium tin oxide (ITO)-coated glass slides, and coverslips for further characterization. Electron microscopy analysis confirmed that the shiny spot was indeed composed of Ag metallic sheets. Figure 1C presents a large area TEM image of an Ag sheet formed on RGO. The size of the deposition spot was influenced by the distance between the spray tip and the deposition surface. An optimal distance of 10–15 mm was consistently maintained during all deposition processes.

The air–water interface plays a critical role in the formation of Ag sheets. The RGO suspension's water component not only contributes to the formation of the RGO layer through electrohydrodynamic motion but also facilitates the removal of unwanted organic residues from the Ag salt precursor. Without the air–water interface, no Ag sheet was formed on a dried RGO spot, deposited on an ITO-coated glass slide (Figure S2, Supporting Information). For this experiment, the RGO suspension was subjected to 30 min of bath sonication and then drop-cast onto an ITO-coated glass slide. The RGO was allowed to dry under laboratory conditions before performing a 2-h ESD of AgOAc. To demonstrate the significance of the RGO thin film formed at the air–water interface through electrohydrodynamic flow in the RGO suspension, an additional control experiment was conducted. In it, 1.5 mL of aqueous RGO suspension was placed in a vial and left open in the laboratory environment. After 3 h, a visible film appeared, floating on the surface. This film was then collected onto an ITO-coated slide and allowed to dry. Subsequently, ESD of Ag salt solution was carried out on the dried spot for a duration of 2 h, followed by SEM imaging. Despite the 2-h-long ESD process, no Ag sheets were observed (Figure S3, Supporting Information). In contrast, the electrohydrodynamic flow enables the tighter packing of RGO layers, as evidenced by the electrical continuity measurement depicted in Figure S1 (Supporting Information).

2.2. Characterization of the Synthesized Ag-Sheets

Figure 2A displays a scanning electron microscopy (SEM) image of Ag sheets formed on an ITO-coated glass slide through 5 h of ESD at a spray current of 100–110 nA. The SEM image reveals that the Ag sheets can cover a large area, with individual sheets reaching sizes of up to 30–35 µm. In Figure 2B, a higher magnification TEM image of a typical Ag sheet is shown. The presence of graphene layers can be clearly observed underneath the Ag sheet, as indicated by the green arrow. In Figure 2C,D, a TEM image of an entire Ag sheet and its corresponding energy-dispersive X-ray spectroscopy (EDS) mapping are presented, respectively. The inset in Figure 2D displays the EDS spectrum collected from the sheet, indicating a composition of 100% Ag. Additionally, the inset in Figure 2C shows an X-ray photoelectron spectroscopy (XPS) spectrum of the Ag sheet. This spectrum confirms the presence of Ag $3d_{5/2}$ at 368.1 eV, providing evidence that the sheets are indeed made of metallic silver.

High-resolution transmission electron microscopy (HRTEM) analysis confirms the crystalline nature of the sheets. **Figure** 3A,B present HRTEM images of the Ag sheet formed on RGO. In Figure 3A, the lattice is clearly visible, with interplanar distances corresponding to the Ag(111) plane. The inset of Figure 3A displays a fast Fourier transform (FFT) image of the single crystalline Ag sheets, showing the cubic close packing of the lattice. Furthermore, careful imaging at the edges of the sheet reveals the presence of RGO layers surrounding the Ag sheets, as shown in Figure 3B. This observation indicates the structural relationship between the Ag sheets and the underlying RGO material.

A thorough investigation using HRTEM was conducted at various locations across the resulting Ag sheet to confirm its single crystalline nature. Figure S4A–C (Supporting Information) depicts HRTEM images showing prominent Ag (111) planes, providing evidence that the Ag sheets are indeed single crystalline. X-ray diffraction (XRD) analysis was also conducted to complement the HRTEM findings. For the XRD experiments, the Ag sheets synthesized were placed on a Si-wafer by careful scooping. Figure 3C presents the XRD spectrum of the Ag sheets on a Si-wafer substrate. The spectrum reveals solely the peak corresponding to the Ag (111) plane at a 2θ value of 38.23°. Figure 3D presents a slow scan spectrum of the Ag (111) region, further confirming the single crystallinity of the Ag sheets formed via ESD. Additionally, the XRD spectrum was collected from the graphene thin film-coated Si-wafer (Figure S5, Supporting Information) as a reference.

2.3. Optimizing Parameters for the Formation of Reproducible and Uniform Ag Sheets

We conducted several experiments to optimize the parameters for achieving reproducible and uniform Ag sheets. These experiments are detailed in this section.

2.3.1. Precursor Salt Concentration

Initially, we varied the concentration of the precursor salt (AgOAc in this case) from 2.5 to 10 m while maintaining a fixed applied potential of 2 kV and a deposition time of 2 h. TEM analysis of the resulting Ag sheets (Figure S6, Supporting Information) revealed significant differences in their crystallinity based on the precursor concentration. At a lower concentration of 2.5 mM (Figure S6A, Supporting Information), the Ag sheets were only partially single-crystalline, indicating incomplete formation. Increasing the concentration to 5 mM (Figure S6B, Supporting Information) led to partial improvement in crystallinity, suggesting a transition toward single-crystallinity but still, the process was incomplete. Utilizing a concentration of 10 mM (Figure S6C, Supporting Information) yielded fully single-crystalline Ag sheets

© 2024 Wiley-VCH GmbH

16136829, 0, Downloaded from https://onlinelibrary.wiley.com/doi/10.1002/smll.202400159 by Central Library, Wiley Online Library on [22/05/2024]. See the Terms and Conditions (https://onlinelibrary.wiley.com/terms-and-conditions) on Wiley Online Library for rules of use; OA articles are governed by the applicable Creative Commons License

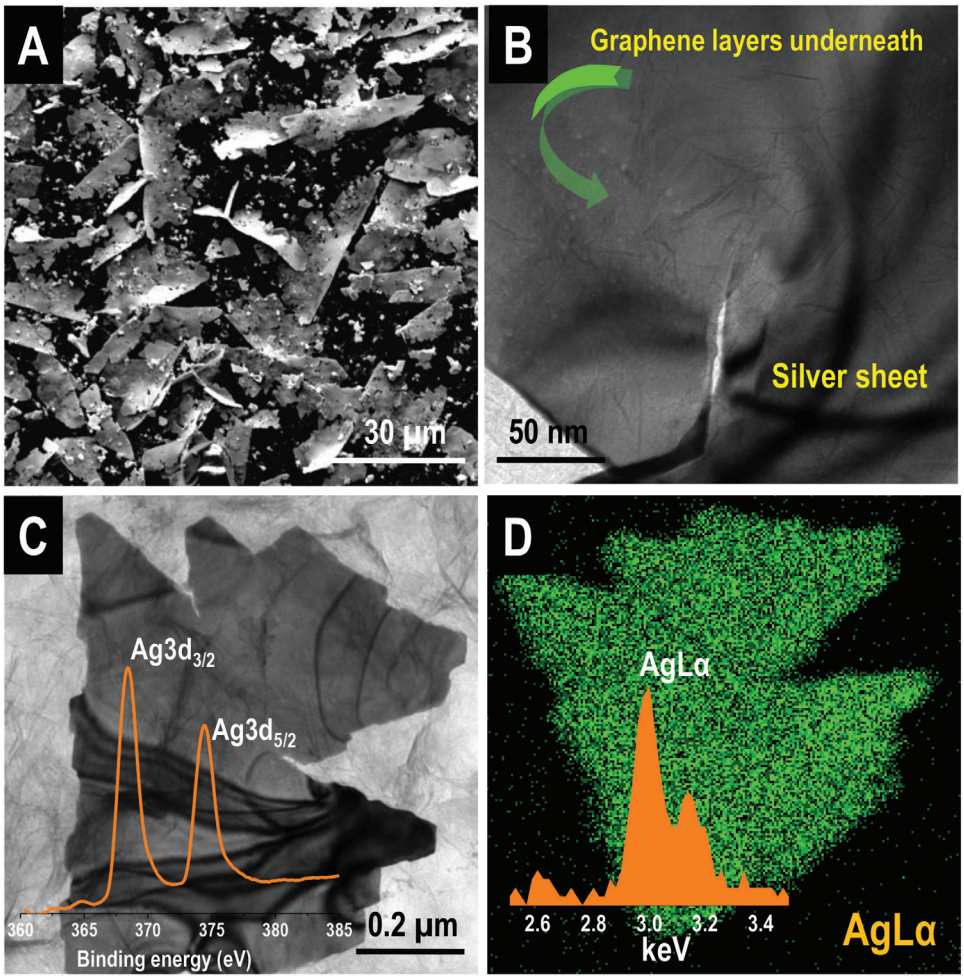

Figure 2. A) SEM image showing Ag sheets synthesized over a large area, B) TEM image of the Ag-sheet revealing its extremely thin nature, with the underlying graphene layers also being observable, C) TEM image showing a large Ag sheet; inset shows an XPS spectrum in the Ag3d region showing that the material is in zero-oxidation state, and D) Energy dispersive spectroscopy (EDS) mapping of the sheet shown in image D; inset of D is the EDS spectrum of the same.

within the 2-h deposition time. This demonstrates the importance of sufficient precursor concentration for achieving complete crystallinity. Based on these findings, we opted for a precursor salt concentration of 10 mM for all the subsequent experiments. Higher concentrations were not explored due to disruptions to the electrospray process caused by high salt content.

2.3.2. RGO Concentration

Upon varying the concentration of RGO in the aqueous suspension, the morphology of the Ag sheets was changed. Figure S7A–C (Supporting Information) showcases TEM images illustrating the Ag sheets formed in an aqueous suspension with different RGO concentrations. At lower RGO concentrations (0.01 wt%), the Ag sheets exhibited a perforated structure. Conversely, an increase in RGO concentration (0.05 wt%) resulted in the formation of solid sheets. This transition is likely attributed to the nonuniform thin film formation (as elaborated earlier, the electrohydrodynamic flow phenomenon leads to the formation of a thin film of RGO on the water surface) at lower RGO concentrations, with regions displaying defects or cracks in the film. These observations underscore the significance of RGO concentration in influencing the characteristics of the sheets.

2.3.3. Time of Deposition

Similarly, we noted that the nature of the sheets was also dependent on the deposition time. Figure S8 (Supporting Information) shows TEM images of Ag sheets formed after different deposition times. It can be observed that as the deposition time increases, the sheets become more solid in nature, whereas those formed at lower deposition times remain perforated. Furthermore, extending the deposition time beyond the formation of solid sheets leads to an increase in the thickness of the resulting sheets (as depicted in Figure 3E,F). To corroborate this observation, we conducted an experiment utilizing two identical ESD setups to synthesize Ag sheets. One setup was operated for 2 h, while the other was allowed to run for 10 h. Figure S9 (Supporting Information)

© 2024 Wiley-VCH GmbH

16136829, 0, Downloaded from https://onlinelibrary.wiley.com/doi/10.1002/smll.202400159 by Central Library, Wiley Online Library on [22/05/2024]. See the Terms and Conditions (https://onlinelibrary.wiley.com/terms-and-conditions) on Wiley Online Library for rules of use; OA articles are governed by the applicable Creative Commons License

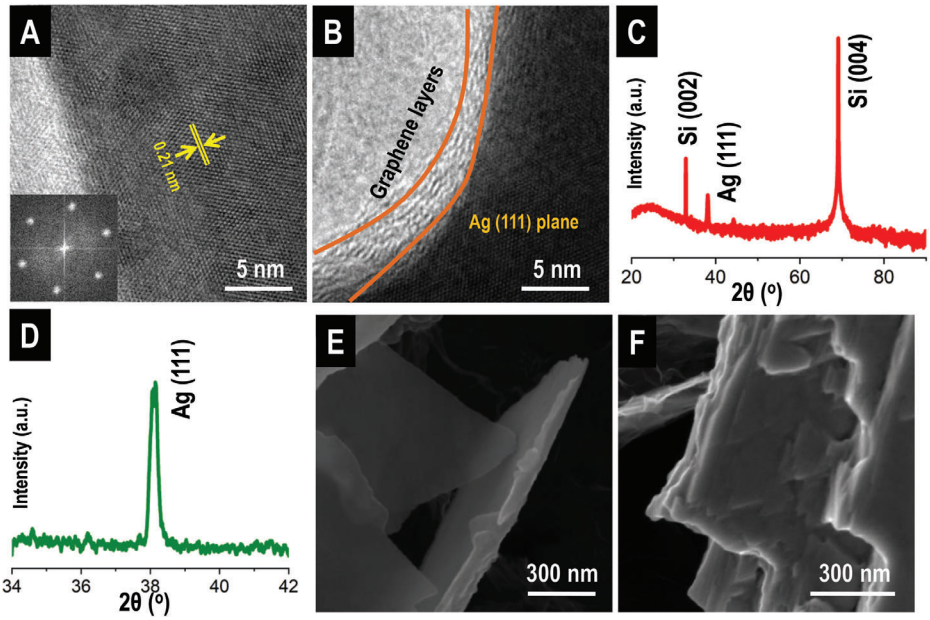

Figure 3. A) HRTEM image of a typical Ag sheet showing Ag (111) plane, these sheets are single crystalline in nature (inset shows the FFT of cubic close packing), B) HRTEM image of an Ag sheet at the edge showing the presence of graphene layers, C) XRD spectrum collected from the as-synthesized Ag sheets, collected over a Si wafer substrate. D) Slow scan XRD spectrum of the Ag (111) region. E) and F) are Field emission scanning electron microscopic (FESEM) images of the Ag sheet showing that these sheets can be very thin or layered in nature depending on the deposition time.

presents FESEM images of the resulting sheets. Notably, the images clearly demonstrate a significant increase in the thickness of the Ag sheets formed during the longer, 10-h deposition process.

2.3.4. Flow Rate, Applied Voltage, and Deposition Rate

It's important to note that another crucial factor influencing the outcome of an ESD process is the deposition rate. A control experiment was performed to investigate the effect of electrospray deposition rate on the synthesized Ag sheets. Two independent experiments were conducted using identical ESD setups except for the deposition rate of the incoming ions. The deposition rate was controlled by monitoring the deposition current using a picoammeter. In one experiment, the current was set at 100 nA (applied voltage 2.0 kV), while 50 nA (applied voltage 1.5 kV) was used in the other. This experiment also demonstrates the effect of flow rate, and different voltages applied for the ESD process as both these parameters are proportional to deposition current. TEM analysis (Figure S10, Supporting Information) of the resulting Ag sheets collected after 1 h of deposition revealed distinct dimensions in the *X*–*Y* plane for each deposition current. This data confirms that the Ag sheets initially grow in a 2D fashion and subsequently begin to increase in thickness with extended deposition times. Therefore, careful control of both the deposition time and rate enables precise tailoring of the sheet size, ultimately leading to the creation of a stable, uniform surface for further applications.

2.3.5. Different Precursor Salts

To investigate the influence of the counter anion on Ag sheet formation on graphene, various silver salt precursors were tested. Ag sheet was formed with all the precursors, including silver acetate, silver perchlorate, and silver nitrate. Figure S11A,B (Supporting Information) present the SEM images of Ag sheets produced using $AgClO_4$ and $AgNO_3$, respectively. These findings reveal that the counter anions have no significant effect on the formation of Ag sheets.

2.4. ESD of Mixtures of Metal Salts

Further, ESD experiments were conducted using mixtures containing different proportions of Ag and Pd precursors to investigate the influence of foreign metal on the Ag sheet formation. In **Figure** 4A,B, TEM images after ESD of the mixture at two different proportions (Ag: Pd 1:1 and 5:1) are shown. Additionally, EDS mapping was performed to determine the presence of the metals. The data presented indicate that there is minimal or no effect of the foreign atom (Pd in this case) on the Ag sheet formation. The formation of Ag sheets appears to be relatively unaffected by the presence of Pd in the precursor mixture.

2.4.1. Extending the Scope of ESD for Metal Separation

We investigated the potential of ESD on graphene for separating metals by depositing mixed precursor solutions. Our initial experiments focused on noble metals, specifically equimolar mixtures of silver with gold and platinum. As depicted in Figure S12 (Supporting Information), the resulting product exhibited clear separation, despite the initial homogenous precursor mixture. Interestingly, silver formed single-crystalline metallic sheets, while the other metals formed distinct nanoparticle assemblies. We further explored this phenomenon using non-noble metal precursors, including a mixture of silver acetate,

© 2024 Wiley-VCH GmbH

16136829, 0, Downloaded from https://onlinelibrary.wiley.com/doi/10.1002/smll.202400159 by Central Library, Wiley Online Library on [22/05/2024]. See the Terms and Conditions (https://onlinelibrary.wiley.com/terms-and-conditions) on Wiley Online Library for rules of use; OA articles are governed by the applicable Creative Commons License

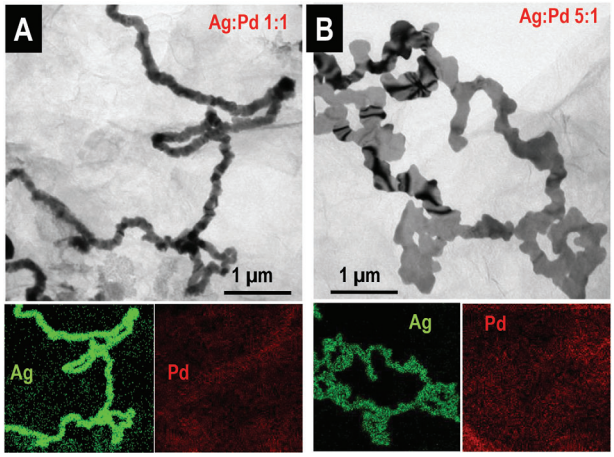

Figure 4. TEM images for ESD of Ag and Pd mixtures: A) Ag: Pd 1:1, and B) Ag: Pd 5:1. Down portions of each figure show EDS maps of the corresponding images.

sodium acetate, and magnesium acetate (representing common hard water contaminants). Figure S13A (Supporting Information) shows an SEM image of the resulting bundle of small Ag sheets. Point EDS analysis (Figure S13B, Supporting Information) confirmed the presence of 100% silver, demonstrating successful separation. Notably, large-area Ag sheets were not observed in this case. This could be attributed to the presence of other metal ions with high mobility occupying the graphene layers, hindering the coalescence of silver. These findings suggest that the ESD method holds promise for effectively separating silver from industrial or mining wastewater. Further research is warranted to explore its applicability to diverse metal-containing waste streams.

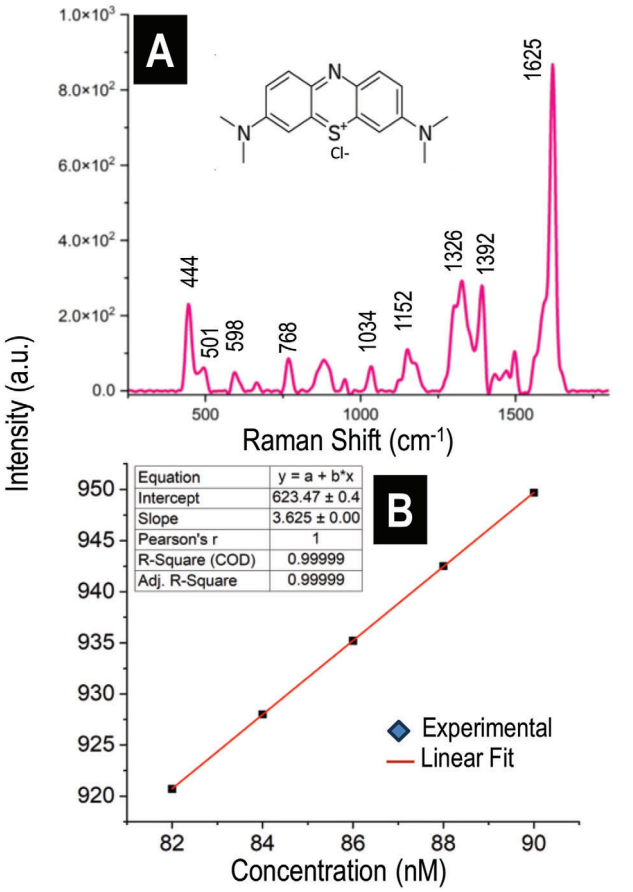

Figure 5. A) Surface-enhanced Raman spectrum of methylene blue, on Ag@RGO surface, B) concentration versus intensity (@1625 cm^{-1}) plot for MB within the concentration range 80–90 nM.

2.5. ESD of Other Noble Metals on Air–Water–Graphene Interface

We tested other noble metals to explore the possibility of forming single crystalline sheets using the same technique. In the case of other noble metals (such as Pd, Au, and Pt) on the aqueous suspension of RGO, the formation of 2D structures was not observed; instead, nanoparticles (size 5–10 nm) were formed. Figures S14 and S15 (Supporting Information) show TEM images of the ESD product of Pd and Au, respectively on RGO. This suggests that further optimization of the conditions is necessary to create sheets. This difference in the structures formed is likely to be due to the nature of the softness of the metals. Ag, being relatively soft compared to Au and Pd, allows for more favorable coalescence of atoms, leading to the formation of 2D structures. However, in the case of Au and Pd, the atoms do not coalesce easily, resulting in the formation of nanoparticles instead of 2D structures.

2.6. Surface-Enhanced Raman Spectroscopy (SERS)

Creating a stable and reliable SERS substrate remains a significant challenge due to factors such as nanoparticle aggregation, metal oxidation, molecule adsorption/desorption dynamics, substrate instability, and reproducibility.[32] This is why stable substrates exhibiting robust SERS properties garner significant attention within the scientific community. In this study, we have successfully fabricated a surface comprised of single-crystalline silver sheets deposited on RGO. These metallic sheets exhibit excellent stability and can be reproducibly formed with controlled sizes. The synergistic interaction between silver and RGO endows the fabricated surface with exceptional SERS capabilities.

Here, we tested the SERS property of the ESD-synthesized Ag sheets embedded in graphene, using methylene blue (MB) as a target molecule (**Figure 5A**). We collected the Raman spectra of various concentrations of MB and constructed a calibration curve to determine the limit of detection. We used the most intense peak for MB at 1625 cm^{-1} for this purpose (Figure 5B and Figure S16, Supporting Information). By employing linear fitting of the data, we evaluated the theoretical limit of detection with an R^2 value of 0.99999. Interestingly, we observed acceptable Raman spectra for MB at concentrations as low as 0.08 μM with the Ag sheets. However, the featured peaks were absent for the same sample with RGO as the substrate (Figure S17, Supporting Information). This observation suggests the synergistic effect of RGO and Ag for SERS-based detection.

© 2024 Wiley-VCH GmbH

16136829, 0, Downloaded from https://onlinelibrary.wiley.com/doi/10.1002/smll.202400159 by Central Library, Wiley Online Library on [22/05/2024]. See the Terms and Conditions (https://onlinelibrary.wiley.com/terms-and-conditions) on Wiley Online Library for rules of use; OA articles are governed by the applicable Creative Commons License

3. Conclusion

A room temperature process to make large area single crystalline Ag sheets from its salt solution, without any other reagent was demonstrated. Although there are multiple studies on enhanced mobility of atoms on graphene surfaces, experimental proof of it was still a challenge due to limitations in experimental design. Here we demonstrated an ambient method that provides a means to test the fate of metal ions/atoms introduced directly on graphene layers. We report that the formation of metal sheets depends on the concentration of reduced graphene oxide suspension and the nature of the metal. The presence of foreign species, such as Pd atoms does not affect the formation of Ag sheets. The method could be used to separate silver from common contaminants such as alkali and alkaline earth metals from solutions. Due to the SERS property of the metals, the method has potential applicability in various fields, including environmental monitoring and biomedical sensing. Our Ag film could detect methylene blue at nanomolar concentrations. The simplicity and sensitivity of the method make our material an attractive candidate for on-site detection applications.

4. Experimental Section

Materials and Methods: All the chemicals used for the experiments were commercially available and were used without any further purification. Silver acetate (AgOAC) and silver perchlorate ($AgClO_4$) were purchased from Sigma–Aldrich, India. $AgNO_3$ was purchased from RANKEM. Reduced graphene oxide (RGO) was chemically synthesized in the laboratory using the modified Hummers' method. Locally available deionized (DI) water was used for making graphene suspension.

Instrumentation: Nanoelectrospray (nESI) emitters were made using a micropipette puller (P-97) purchased from Sutter Instrument, USA. Transmission electron microscopy (TEM) and high-resolution transmission electron microscopy (HRTEM) were performed using an accelerating voltage of 200 kV using a JEOL 3010, 300 kV instrument equipped with a UHR polepiece. A Gatan 794 multiscan CCD camera was used for image acquisition. EDS spectra were collected on the Oxford Semistem system housed on the TEM. Samples were taken onto 300-mesh carbon-coated copper grids (spi Supplies, 3530C-MB) by dipping them into a graphenic suspension after Ag deposition and drying under ambient conditions before examining them in TEM. A field emission scanning electron microscope (FEI Quanta FEG 200, USA) was used to image the Ag sheets. Energy dispersive spectroscopy (EDS) analyses were performed with the same SEM instrument. Some images were collected also with an FEI Quanta 100 instrument having a tungsten filament source. X-ray photoelectron spectroscopic (XPS) measurements were conducted using an Omicron ESCA probe spectrometer with polychromatic MgKα X-rays ($h\nu = 1253.6$ eV). Raman measurements were made using a Confocal Raman micro spectrometer (Witec GmbH, Germany) with 532 and 633 nm laser sources.

Synthesis of Graphene: Reduced graphene oxide (RGO) was synthesized using the modified Hummers' method. 25 mL concentrated sulphuric acid (H_2SO_4), 5 g potassium persulfate ($K_2S_2O_8$), and 5 g of phosphorus pentoxide (P_2O_5) were mixed in a 250 mL beaker and heated at 90 °C with continuous stirring till all the reagents dissolved in H_2SO_4. Then the temperature of the reaction mixture was brought down to 80 °C, and 6 g of graphite powder was added slowly to it. The temperature of the reaction mixture was maintained at 80 °C for 5 h. Bubbling in the reaction mixture was observed initially, which was subsidized with time. After 5 h of heating the reaction mixture was kept for cooling at room temperature. Once it was cooled, it was diluted with 1 L of distilled water and kept undisturbed overnight. The resultant solution was filtered, and the supernatant was washed thoroughly with water to remove excess acid present in it.

About 230 mL of concentrated H_2SO_4 was taken in a 500 mL beaker and it was maintained at 0–5 °C by keeping it in an ice bath. Then the pre-oxidized graphite was added to the cooled acid with stirring. ≈15 g of potassium permanganate ($KMnO_4$) was carefully added to this mixture. The addition of $KMnO_4$ was done such that the temperature of the mixture did not go beyond 10 °C. Then this reaction mixture was kept at 35 °C for 2 h. Once the reaction was complete, 1 L of distilled water was added to the mixture very carefully so that the temperature did not go beyond 50 °C. After the addition of water, the mixture was kept for stirring for another 2 h. Afterward, 1.5 L of distilled water and 25 mL of 30% H_2O_2 were added to it. Then it was kept at room temperature for one day. The supernatant was discarded slowly and the remaining solution was centrifuged and repeatedly washed with 10% HCl followed by water. Then the resultant solid was dried in air and 2% (w/v) water dispersion was made, and it was dialyzed for 3 weeks continuously to remove contaminants like salts and acid. After dialysis, the dispersion was diluted to obtain 0.5% (w/v) graphene oxide (GO).

The GO dispersion was then reduced to get RGO. Pre-reduction of GO was done by adding sodium carbonate (5 wt%) and 800 mg of sodium borohydride followed by heating for 1 h. Then the reaction mixture was cooled, centrifuged, and washed with water thoroughly and redispersed. To make a free-standing dispersion of RGO in water, sulfonation was done. For that 20 mg sulfanilic acid and 8 mg sodium nitrite were dissolved in 0.25% NaOH solution followed by the addition of 4 mL 0.1 M HCl. Then the mixture was stirred and kept in an ice bath. After 15 min of stirring, aryl diazonium salt solution was added to 20 mL, 0.5 mg mL^{-1} RGO dispersion. Then the reaction mixture was kept in an ice bath and stirred for 2 h. After the reaction was complete, it was filtered washed with water repeatedly, and redispersed to obtain 0.05 wt% RGO suspension.

Electrospray Deposition (ESD): Spray emitters for ESD were made using a borosilicate glass capillary of 0.86 mm inner diameter and 1.5 mm outer diameter. The glass capillaries were pulled in such a way that they had an opening of 10–25 µm at the tip. Each tip underwent quality control through optical microscopy, and any deviation from the desired size range or exhibiting flaws was discarded. This specific size range was chosen based on previous findings, where it was shown to be crucial for achieving long-term stability for ESD.[6,7,33,34] Selected tips were filled with an aqueous solution (10 mM) of silver acetate (AgOAc) using a microinjector pipette tip. It was then connected to a homemade electrode assembly. A positive voltage in the range 2–2.5 kV was applied through a platinum wire. With the application of the high voltage, a spray plume containing the charged droplets was visible at the tip of the sprayer. This spray plume was directed to an Eppendorf tube containing an aqueous suspension of RGO. To have a stable continuous spray, the liquid was grounded by pasting a copper strip on the inner wall of the vial. The deposition current was maintained at 100–110 nA using a picoammeter. The details are presented in the inset of Figure 1A.

Supporting Information

Supporting Information is available from the Wiley Online Library or from the author.

Acknowledgements

The authors acknowledge DST, Govt. of India, and IIT Madras for research funding. The authors acknowledge Dr. Bivas Saha and Mr. Debmalya Mukhopadhyay of JNCSAR, Bengaluru for helping in measuring the XRD data.

Conflict of Interest

The authors declare no conflict of interest.

© 2024 Wiley-VCH GmbH

16136829, 0, Downloaded from https://onlinelibrary.wiley.com/doi/10.1002/smll.202400159 by Central Library, Wiley Online Library on [22/05/2024]. See the Terms and Conditions (https://onlinelibrary.wiley.com/terms-and-conditions) on Wiley Online Library for rules of use; OA articles are governed by the applicable Creative Commons License

Author Contributions

D.S. was responsible for the conception and design of the work, data collection, data analysis and interpretation, drafting, and editing of the article. A.S. performed TEM measurements, data analysis and interpretation, drafting, and editing of the article. K.U. performed electrospray deposition. S.M. performed Raman measurements. T.P. supervised the study, performed data analysis, interpretation of results, and editing of the article.

Data Availability Statement

The data that support the findings of this study are available from the corresponding author upon reasonable request.

Keywords

ambient ions, electrospray deposition, graphene, microdroplets, SERS, silver sheets

Received: January 8, 2024
Revised: March 26, 2024
Published online:

[1] G. Siuzdak, T. Hollenbeck, B. Bothner, *J. Mass Spectrom.* **1999**, *34*, 1087.
[2] M. K. Rahman, T. H. Phung, S. Oh, S. H. Kim, T. N. Ng, K.-S. Kwon, *ACS Appl. Mater. Interfaces.* **2021**, *13*, 18227.
[3] V. N. Morozov, *Adv. Biochem. Eng. Biotechnol.* **2010**, *119*, 115.
[4] V. N. Morozov, T. Y. Morozova, *Anal. Chem.* **1999**, *71*, 1415.
[5] J. Ghosh, R. G. Cooks, *Trends Analyt. Chem.* **2023**, *161*, 117010.
[6] D. Sarkar, M. K. Mahitha, A. Som, A. Li, M. Wleklinski, R. G. Cooks, T. Pradeep, *Adv. Mater.* **2016**, *28*, 2223.
[7] D. Sarkar, R. Singh, A. Som, C. K. Manju, M. A. Ganayee, R. Adhikari, T. Pradeep, *J. Phys. Chem. C.* **2018**, *122*, 17777.
[8] R. Dong, T. Zhang, X. Feng, *Chem. Rev.* **2018**, *118*, 6189.
[9] H.-S. Jang, B. Seong, X. Zang, H. Lee, J. W. Bae, D.-H. Cho, E. Kao, C. Yang, G. Kang, Y. Liu, H. S. Park, D. Byun, L. Lin, *Adv. Mater. Interfaces.* **2018**, *5*, 1701491.
[10] Y. Zhang, Y.-W. Tan, H. L. Stormer, P. Kim, *Nat. Plants.* **2005**, *438*, 201.
[11] A. H. Castro Neto, F. Guinea, N. M. R. Peres, K. S. Novoselov, A. K. Geim, *Rev. Mod. Phys.* **2009**, *81*, 109.
[12] X. Du, I. Skachko, A. Barker, E. Y. Andrei, *Nat. Nanotechnol.* **2008**, *3*, 491.
[13] O. C. Compton, S. T. Nguyen, *Small.* **2010**, *6*, 711.
[14] X. Zhao, Q. Zhang, D. Chen, P. Lu, *Macromolecules.* **2010**, *43*, 2357.
[15] L.-C. Tang, Y.-J. Wan, D. Yan, Y.-B. Pei, L. Zhao, Y.-B. Li, L.-B. Wu, J.-X. Jiang, G.-Q. Lai, *Carbon.* **2013**, *60*, 16.
[16] F. Bonaccorso, Z. Sun, T. Hasan, A. C. Ferrari, *Nat. Photonics.* **2010**, *4*, 611.
[17] W. Zhou, M. D. Kapetanakis, M. P. Prange, S. T. Pantelides, S. J. Pennycook, J.-C. Idrobo, *Phys. Rev. Lett.* **2012**, *109*, 206803/1.
[18] O. Cretu, A. V. Krasheninnikov, J. A. Rodriguez-Manzo, L. Sun, R. M. Nieminen, F. Banhart, *Phys. Rev. Lett.* **2010**, *105*, 196102/1.
[19] W. D. Luedtke, U. Landman, *Phys. Rev. Lett.* **1999**, *83*, 1702.
[20] B. Yoon, W. D. Luedtke, J. Gao, U. Landman, *J. Phys. Chem. B.* **2003**, *107*, 5882.
[21] C. Zheng, W. Chen, Y. Huang, X. Xiao, X. Ye, *RSC Adv.* **2014**, *4*, 39697.
[22] B. Wang, B. Yoon, M. Koenig, Y. Fukamori, F. Esch, U. Heiz, U. Landman, *Nano Lett.* **2012**, *12*, 5907.
[23] S. S. Chae, S. Jang, W. Lee, D. W. Jung, K. H. Lee, J. D. Kim, D. Jeong, H. Chang, J. Y. Hwang, J.-O. Lee, *Small.* **2018**, *14*, 1801529.
[24] I. Shtepliuk, I. G. Ivanov, N. Pliatsikas, T. Iakimov, S. Lara-Avila, K. H. Kim, N. Ben Sedrine, S. E. Kubatkin, K. Sarakinos, R. Yakimova, *ACS Appl. Nano Mater.* **2021**, *4*, 1282.
[25] A. Ghosh, T. Pradeep, J. Chakrabarti, *J. Phys. Chem. C.* **2014**, *118*, 13959.
[26] C. P. Johnson, *Thin Film Process.* **1991**, *II*, 209.
[27] I. G. Brown, *Annu. Rev. Mater. Res.* **1998**, *28*, 243.
[28] N. Ghobadi, S. Rezaee, *J Mater Sci Mater Electron.* **2016**, *27*, 8464.
[29] P. Asanithi, S. Chaiyakun, P. Limsuwan, *J. Nanomater.* **2012**, *2012*, 963609.
[30] X. Yan, *Int. J. Mass Spectrom.* **2021**, *468*, 116639.
[31] A. B. Theberge, F. Courtois, Y. Schaerli, M. Fischlechner, C. Abell, F. Hollfelder, W. T. S. Huck, *Angew. Chem., Int. Ed.* **2010**, *49*, 5846.
[32] J. Prakash, *Int. Rev. Phys. Chem.* **2019**, *38*, 201.
[33] D. Sarkar, B. Mondal, A. Som, S. J. Ravindran, S. K. Jana, C. K. Manju, T. Pradeep, *Glob. Chall.* **2018**, *2*, 1800052.
[34] D. Sarkar, A. Som, T. Pradeep, *Anal. Chem.* **2017**, *89*, 11378.

© 2024 Wiley-VCH GmbH

16136829, 0, Downloaded from https://onlinelibrary.wiley.com/doi/10.1002/smll.202400159 by Central Library, Wiley Online Library on [22/05/2024]. See the Terms and Conditions (https://onlinelibrary.wiley.com/terms-and-conditions) on Wiley Online Library for rules of use; OA articles are governed by the applicable Creative Commons License